

ITB formation in terms of $\omega_{E \times B}$ flow shear and magnetic shear s on JET

T J J Tala¹, J A Heikkinen¹, V V Parail², Yu F Baranov² and S J Karttunen¹

¹ Association Euratom-Tekes, VTT Chemical Technology, PO Box 1404, FIN-02044 VTT, Finland

² EURATOM/UKAEA Fusion Association, Culham Science Centre, Abingdon, OX14 3EA, UK

Received 2 November 2000, in final form 29 January 2001

Abstract

A linear empirical threshold condition $\omega_{E \times B} / \gamma_{ITG} > 0.68s - 0.095$ has been found for the onset of the ion internal transport barriers in the JET optimised shear database. Here, s is the magnetic shear, $\omega_{E \times B}$ the flow shearing rate and γ_{ITG} is an approximate of the linear growth rate of the ion temperature gradient instability. The present empirical threshold condition for the ITB formation will provide a first clear indication of the strong correlation of s and $\omega_{E \times B}$ at the ITB transition. The empirical analysis consists of ITB discharges from a wide plasma parameter range; the toroidal magnetic field varies between 1.8–4.0 T, the auxiliary heating power between 10–30 MW and the diamagnetic energy between 3–12 MJ. The predictive simulations of several ITB discharges with the empirical ITB threshold condition reproduce the experiments with time averaged prediction errors of the order of 10–25% in T_i and T_e profiles and 10–15% in n_e profiles as well as the toroidal flow velocity with errors of the order of 10–20%. The simulated times of the onset of the ITB compared to the experimental ones are typically within 0.4 s and the simulated ITB widths within 0.1 in r/a throughout the whole simulations.

1. Introduction

Internal transport barriers (ITBs) have now been recognized as having the potential to operate fusion machines in an improved confinement mode where the pressure gradients can drive the required bootstrap current [1, 2, 3, 4]. At present, there is an urgent need to understand the parameter dependence of the threshold for the ITB formation, the dynamics of the barrier and the collapse of the barrier.

The physical mechanism of the ITB formation has not yet been clearly identified. The $\omega_{E \times B}$ flow shear is commonly regarded as a very crucial factor in the ITB formation in most theories [5, 6, 7] and also found to be important in most ITB experiments on different tokamaks [8, 9, 10, 11]. Another crucial factor possibly contributing to the ITB formation is the weak or negative magnetic shear in the plasma core region, demonstrated also on many

tokamaks [1, 12, 13, 14]. The combined effects of $\omega_{E \times B}$ velocity shear and magnetic shear s on turbulence suppression and transport in magnetic confinement devices have been investigated in [15]. A third possible factor affecting the ITB formation are the low order rational q -surfaces, reported on JET and RTP in [16, 17, 18]. Other explanations for the ITB formation consider Shafranov-shift-induced turbulence stabilization [19] and turbulence suppression by the turbulence generated zonal flows [20]. The role of the inhomogeneity in the plasma, i.e. the ion temperature gradient (ITG) and electron temperature gradient (ETG) modes can be of major significance. The possible mechanisms listed above are not independent of each other and most probably, the ITB formation is an interplay of two or more physical mechanisms.

ITBs have been identified either separately in the ion and electron channels or, as is often the case, with both ion and electron transport suppression occurring at the same barrier position, although not necessarily simultaneously [21]. Typically on JET after the onset of the ITB, χ_e drops approximately by a factor of 5 while χ_i falls by more than an order of magnitude, almost to the neo-classical level in the plasma core. In the absence of any satisfactory theory that is based on the first principles for the onset of the ITB, empirical predictive transport models describing the suppression of the microturbulence and the further evolution of the ITB have been developed [22, 23, 24]. Here, the standard transport equations for the ion and electron temperatures, density, flow velocities and magnetic flux as well as various types of turbulence models have been amended by the inclusion of an ITB transition model. In [23], the ITB transition has been described as a jump from ELMy H mode or L mode to an improved core confinement with a linear combination of a Hahn–Burrell flow shearing rate $\omega_{E \times B}$ [25] and magnetic shear. An alternative method to the Hahn–Burrell flow shear model takes into account the effect of the weak magnetic shear in addition to $\omega_{E \times B}$ flow shear mechanism. There one has introduced a flow shearing rate factor which is called the Hamaguchi–Horton shear parameter [26]. This has been used in the simulation of ITBs in [22], taking also into account the magnetic shear effect as presented in Weiland model in [27]. Various numerical techniques in order to allow time-dependent transport codes to dynamically follow bifurcations to enhanced confinement regimes by self-consistently computing the effect of $E \times B$ shear stabilization are investigated in [24].

In this paper, the $\omega_{E \times B}$ flow shear and the magnetic shear s are determined from the JET optimized shear (OS) experiments at the ITB transition. These values are used to construct an empirical ITB transition threshold condition in terms of the shear quantities $\omega_{E \times B}$ and s . This empirical condition is further employed in predictive simulations to describe the ITB onset, evolution and a possible collapse. The present empirical fit of s and $\omega_{E \times B}$ for the ITB transition provides the first clear indication of the strong correlation of s and $\omega_{E \times B}$ at the ITB transition. It will be further shown that the statistical error in the fit reduces significantly if instead of $\omega_{E \times B}$ flow shear a quantity $\omega_{E \times B}/\gamma_{ITG}$ is used. This indicates the significant role of ITG turbulence in the ITB formation in JET. $\gamma_{ITG} = v_{th}/L_T$ approximates the linear growth rate of the ITG type of plasma turbulence, where $v_{th} = \sqrt{2k_B T_i/m_i}$ is the ion thermal velocity with T_i being the ion temperature and m_i the ion mass, and $L_T = T_i/(\partial T_i/\partial R)$ is the ion temperature scale length.

In finding the values of s and $\omega_{E \times B}$ at the ITB transition from the experimental data, special attention must be paid to determining the location and time of the onset of the ITB. This is complicated by the limited accuracy in spatial and temporal resolution of the charge exchange spectroscopy (CXs) (temporal resolution ≈ 50 ms, spatial resolution ≈ 10 cm), electron cyclotron emission (ECE) and magnetic measurements. Motional Stark effect (MSE) measurements are not available for the JET OS discharges considered in this analysis and, as a consequence, the magnetic shear calculated by EFIT [28] without MSE measurements has large error bars. Therefore, s is inferred from interpretative JETTO [29] simulations,

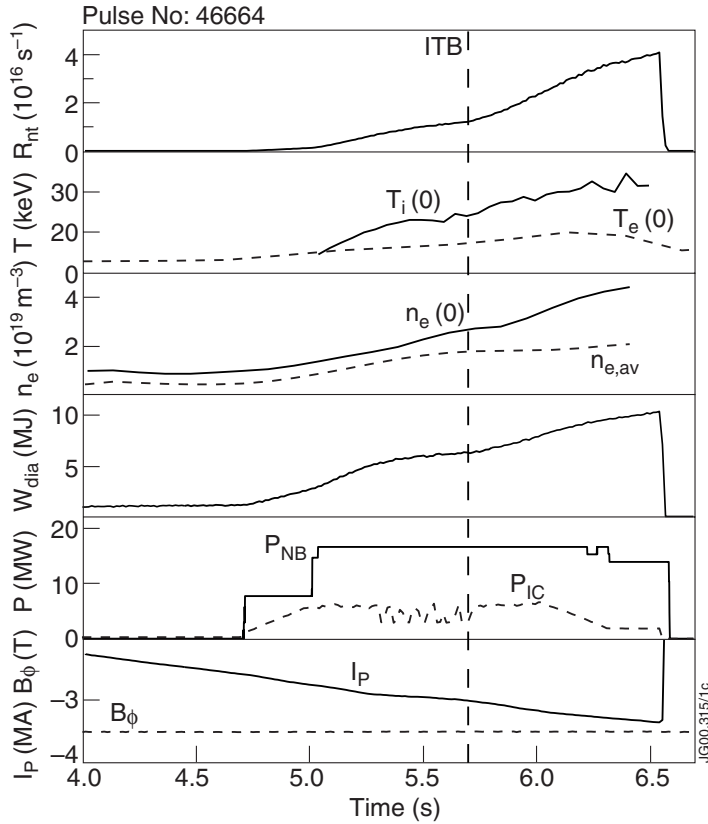


Figure 1. Time traces of the neutron rate R_{nt} , the central ion T_i and electron T_e temperatures, the central and volume averaged electron density n_e , the diamagnetic energy W_{dia} , the heating powers P_{NB} and P_{IC} and the plasma current I_p and toroidal magnetic field B_ϕ for the OS discharge pulse No 46664. ITB appears at $t = 5.6$ s (shown by the vertical dashed line) and L–H mode transition occurs after $t = 5.1$ s.

i.e. only Faraday’s equation is solved for the current by using the neo-classical conductivity and external sources for current, but all the other quantities (temperatures, densities, plasma current, toroidal magnetic field, Z_{eff} , etc.) are taken from the experiment. The time for the onset of the ITB is inferred from the sudden increase in the $\tau_{ITER-97}$ confinement time. The possibility of the increase in the confinement time being due to the L–H transition can be excluded by checking the D_α signal. After determining the time for the onset of the ITB, the radial location is inferred from the large gradients in the temperature profiles. A dimensionless criterion for characterising ITBs was reported very recently in [30]. That method, also based on the similar determination of the temperature gradients, is not used here, but it gives similar results.

Figure 1 shows time traces of typical plasma parameters from a $B_\phi = 3.4$ T, $I_p = 3.4$ MA (peak) OS discharge No 46664. This pulse was selected because it has a very strong and clear ITB formation, both in time and space, and also the time evolution of the ITB can be tracked with small experimental errors. The ITB forms at $t = 5.6$ s and this can be seen as a sudden increase in R_{nt} signal at the same time in figure 1. The discharge ends up with a disruption due to the emergence of a pressure driven kink instability at $t = 6.5$ s.

The paper is structured in the following way. Section 2 illustrates the calculation of the

radial electric field E_r and its different components with and without ITBs in JET. In section 3, the ITB formation is studied in terms of $\omega_{E \times B}$ shearing rate and magnetic shear s . An empirical threshold condition for the ITB formation is found. That empirical ITB transition condition is applied in predictive simulations to an extensive set of JET OS plasmas in section 4. The maximum simulation errors in T_i , T_e , n_e and the toroidal rotation velocity v_ϕ as well as ITB formation time and location are also estimated. Finally, we summarize and discuss the results in section 5.

2. Calculation of the radial electric field E_r

The radial electric field for the main plasma ions is calculated as follows:

$$E_r = \frac{1}{Zen_i} \frac{\partial p_i}{\partial r} - v_\theta B_\phi + v_\phi B_\theta, \quad (1)$$

where v_θ and v_ϕ are the poloidal and toroidal velocities and B_θ and B_ϕ the poloidal and toroidal magnetic fields, respectively, n_i is the ion density, Z is the ion charge number and e the elementary charge. Experimentally measured values for all other quantities except v_θ are available in the calculation of E_r , and due to the lack of measurements of v_θ in JET, it is assumed to be neo-classical. The validity of this assumption has been discussed in [31] and it was concluded that anomalous viscosity can be neglected compared to neo-classical viscosity provided that the typical scale length of the poloidal rotation is much longer than the poloidal Larmor radius of the ions. Within the present model for v_θ , we do not consider either ripple- or turbulence-originated sources of torque for poloidal rotation, although such mechanisms may play a role in the ITB formation in some configurations [20, 32]. Toroidal rotation velocity v_ϕ is measured by charge exchange spectroscopy using the carbon impurity. The difference between the toroidal rotation of the carbon impurity and the main ion for plasmas with NBI (large momentum input) is found to be at most of the order of 10–15% at radii where the ITBs take place. The correction has been calculated with an equation given in [33].

The radial electric field and its different components are shown 0.6 s before the ITB transition in figure 2 (a) and 0.6 s after the ITB formation in figure 2 (b) for the JET discharge No 46664. The contribution from the toroidal rotation (dash-dotted curve) is clearly dominant in the total E_r (thick solid), both before and after the ITB formation. The dominance of $E_{r,\phi} = v_\phi B_\theta$ in E_r becomes even more pronounced because the poloidal velocity term $E_{r,\theta} = v_\theta B_\phi$ (dotted curve) almost cancels out the pressure gradient term $E_{r,\nabla p} = \frac{1}{Zen_i} \frac{\partial p_i}{\partial r}$ (dashed curve), the difference being indicated also in figure 2. The partial cancellation of these two terms is a direct consequence of the used neo-classical model for v_θ in the banana-regime. The magnitude of E_r and its all components are about 5 times larger after the formation of the ITB than before it. The footpoint of the ITB is at $\rho \approx 0.56$ in figure 2 (b). The values for E_r and its different components are found to be of the same order of magnitude and follow the same qualitative behaviour for other JET OS discharges as well.

In JET, the toroidal rotation produced mainly by the co-rotating neutral beam injection (NBI) always gives a positive contribution to E_r as illustrated in figure 2. For co-injected NBI, the dominant contribution from the toroidal rotation term $E_{r,\phi}$ to the radial electric field and its gradient is reduced by the sum of the two remaining terms, i.e. pressure gradient and poloidal rotation terms as $(E_{r,\nabla p} - E_{r,\theta})$. Then if the pressure gradient is increased, E_r and its gradient is decreased, thus hindering the formation and expansion of the ITB. However, in the case of counter-injection the toroidal rotation term and the remaining two terms add to each other, increasing E_r with increasing pressure gradient. Consequently, there is a reason to expect that the ITBs would be wider for discharges with the counter-injected NBI because increasing the

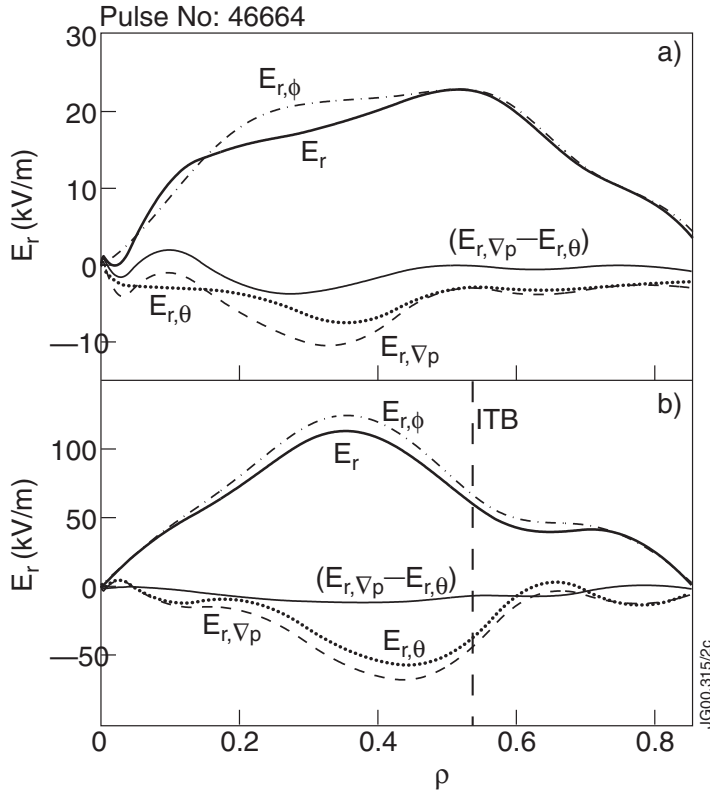


Figure 2. E_r and its components 0.6 s before (a) and 0.6 s after (b) the ITB formation as a function of $\rho = \sqrt{\Phi/\pi B_\phi}/a_{\text{eff}}$ with a_{eff} being the radius of the circle covering the same area as the elongated plasma for JET pulse No 46664. The footpoint of the ITB is shown by the vertical dashed line in (b).

gradient of the radial electric field will reinforce the positive effect of $\omega_{E \times B}$ shearing rate on the turbulence suppression and further on the ITB formation. In addition, the counter-injected current in the plasma core produced by NBI could help in decreasing the magnetic shear in the plasma centre, thus further facilitating wider ITBs.

Theoretically counter-momentum injection was predicted to lower the power threshold to form an ITB and produce a wider ITB in [34]. Experimentally NBI counter-injection was demonstrated to be better at sustaining the ITB compared to co-injection on TFTR [19, 36]. However, balanced-injection turned out to be enough or even better to sustain and form an ITB on TFTR when the magnetic shear was negative in the core plasma. The advantage of balanced-injection in reversed shear (RS) plasmas was also reported in JT-60U [9]. In DIII-D negative central shear (NCS) plasmas, discharges with NBI counter-injection exhibited wider ITBs compared to those with co-injection [35]. NBI co-injection produced a positive E_r hill which then gradually lead to the formation of relatively narrow ITBs with a very small power threshold whereas with counter-injection, wider ITBs were obtained but with a higher power threshold [35, 36]. In addition, the recently found promising steady state operating mode, so-called quiescent double barrier (QDB) mode requires necessarily a counter NBI [37]. When comparing the time behaviour and the profiles of the different components of the radial electric field before and after the ITB formation between different tokamaks, DIII-D plasmas with NBI

co-injection are found to remind most of the present situation on JET.

To actively control the width and strength of the ITB, a flexible NBI system is needed. Recent results from JT-60U indicate that changing the toroidal momentum injection, i.e. toroidal rotation, by changing from co- to balanced or counter-injection or vice versa, the width and strength of the ITB can be controlled [38].

3. $\omega_{E \times B}$ flow shear versus magnetic shear s in ITB formation

The $\omega_{E \times B}$ shearing rate is calculated following [25]

$$\omega_{E \times B} = \left| \frac{RB_\theta^2}{B_\phi} \frac{\partial}{\partial \Psi} \frac{E_r}{RB_\theta} \right|, \quad (2)$$

where Ψ is the poloidal flux, R the major radius and E_r calculated as in section 2. In figure 3, we plot 13 ITB pulses in H mode, 3 ITB pulses in L mode and 3 pulses where no ITB was observed for the ITB formation threshold condition of JET optimized shear discharges. The plasma parameter range of the analysed pulses is very wide, i.e. B_ϕ varies between 1.8–4.0 T, the input power in the range 10–30 MW and the diamagnetic energy in the range 3–12 MJ among the investigated pulses. The magnetic shear s , calculated in an interpretative way by JETTO [29], is presented before and after the ITB formation as a function of $\omega_{E \times B}$ in figure 3. The diamonds denote the values of s and $\omega_{E \times B} \sim 50$ ms before the ITB formation and the stars ~ 50 ms after it for OS pulses with ELMy H-mode edge. For L-mode plasma edge discharges, the triangles symbolize s and $\omega_{E \times B} \sim 50$ ms before the ITB transition and the plus signs ~ 50 ms after the transition. The reason for using the instants ~ 50 ms before or after the ITB formation is the temporal resolution (50 ms) from CXS measurements for T_i and v_ϕ . The values of s and $\omega_{E \times B}$ are taken at the location of the footpoint of the ITB. Thus, there are two sets of pairs that belong to the same discharge, i.e. each diamond has a corresponding star that has originated from the same discharge, calculated ~ 100 ms later after the onset of the ITB (H mode), and each triangle has a corresponding plus-sign that has come from the same discharge (L mode) in a similar way. For the three discharges marked with circles, no ITB was observed. In these cases, the values of s and $\omega_{E \times B}$ are taken at the most likely location and instant for an ITB to take place. There are also three back transitions from an ITB state back to an ELMy H-mode plasma included in the ITB transitions presented in figure 3.

There seems to be a trend in figure 3 that larger values of the magnetic shear require a larger $\omega_{E \times B}$ shearing rate for an ITB to be formed. This trend can be seen as all the points with larger s tend to be located more on the right-hand side, thus indicating larger $\omega_{E \times B}$ to be needed to trigger the ITB for those cases. Also, there seems to be another trend in figure 3, an obvious separation of diamonds and stars (H-mode discharges) and triangles and plus signs (L mode discharges), i.e. values of $\omega_{E \times B}$ and s are different before and after the appearance of the ITB. This separation is mainly horizontal, indicating that the $\omega_{E \times B}$ shearing rate increases significantly within 100 ms time interval around the ITB formation whereas the magnetic shear remains almost unchanged at the same time. In order to see whether the trend is clearer when taking into account the turbulence growth rate we define a dimensionless ratio of the $\omega_{E \times B}$ shearing rate to the maximum linear growth rate of the ITG type of plasma turbulence γ_{ITG} , $\Omega = \omega_{E \times B} / \gamma_{ITG}$ where the linear ITG instability growth rate is $\gamma_{ITG} \propto v_{i,th} / R$ with $v_{i,th}$ being the ion thermal velocity. To reach the maximum accuracy for the estimation of the growth rates, more sophisticated models for the calculation of the ITG turbulence, such as Weiland's model [27, 39], should be used, but within the scope of this simplified empirical work we will use only the simplified expression. Inclusion of the Weiland's turbulence model is left for future work.

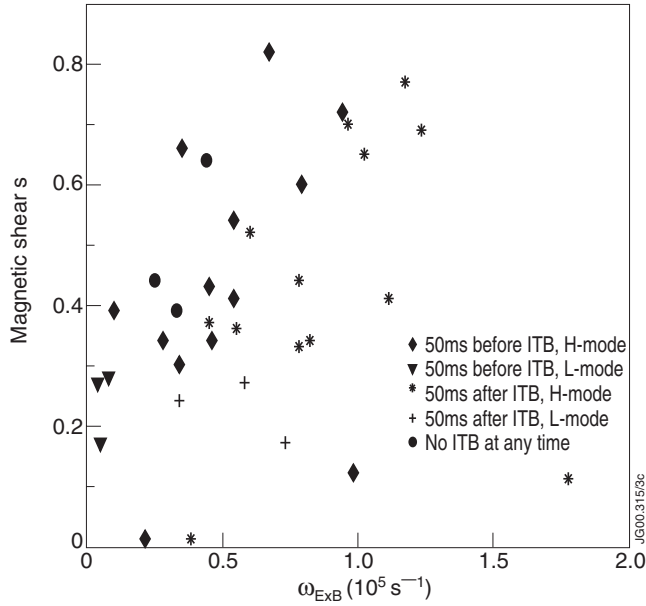


Figure 3. Magnetic shear and $\omega_{E \times B}$ at the ITB location for the ITB formation threshold condition.

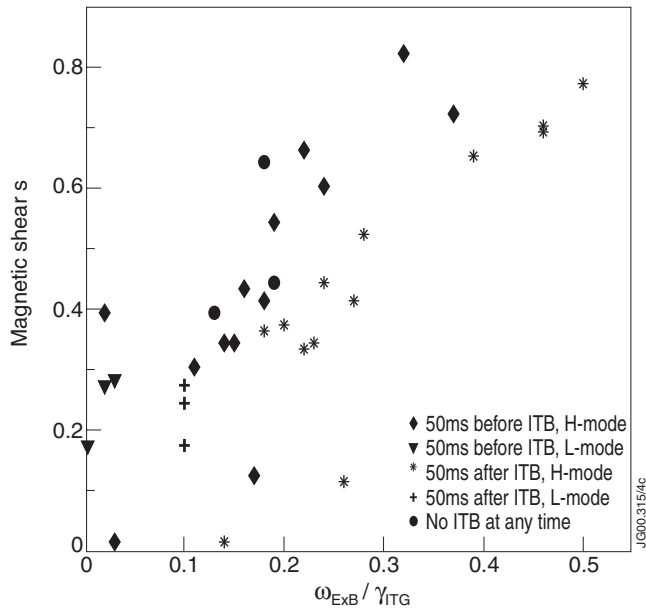


Figure 4. As in figure 3, but $\omega_{E \times B}$ shearing rate is divided by the ITG instability growth rate γ_{ITG} (x axis).

Figure 4 illustrates again the same ITB pulses for ITB formation threshold conditions, with the only exception that now $\omega_{E \times B}$ flow shear is divided by the ITG instability growth rate γ_{ITG} . Now the separation of the discharges before the ITB formation (diamonds in H mode and triangles in L mode) and after the formation (stars in H mode and plus signs in L mode) is more

systematic than without dividing $\omega_{E \times B}$ by γ_{ITG} as presented in figure 3. As a consequence, this can be regarded also as an indirect indication that the ITG turbulence and the ITG turbulence suppression play a major role in the ITB formation process with these JET OS discharges.

Since measurements of T_i and v_ϕ are not always available at the instant of the ITB formation because of the temporal resolution of CXS diagnostic, we will estimate more accurate values for the shear quantities (s and $\omega_{E \times B}$) at the onset of the ITB. The procedure takes the mid-point of each two points that belong to the same discharge in figures 3 and 4, i.e. linear interpolation of the points that are definitely before (~ 50 ms) and definitely after (~ 50 ms) the ITB formation. The resulting mid-points then depict the shear quantities at the onset of the ITB within the experimental measurement accuracy in the s - $\omega_{E \times B}$ and in the s - Ω spaces. Figure 5 presents the values of s and $\omega_{E \times B}$ in figure 5(a) and s and Ω in figure 5(b) for the same discharges as in figures 3 and 4, respectively. Naturally, the three discharges with no ITB are excluded in figure 5.

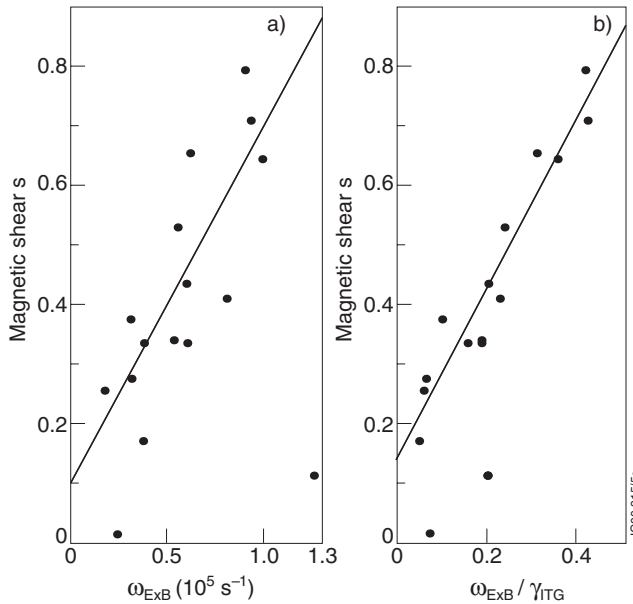


Figure 5. As in figures 3 and 4, but linearly interpolated values for s , $\omega_{E \times B}$ and Ω are used. Shown also are the straight lines, i.e. the best fits calculated with the least-squares method.

Both scatter plots in figure 5 exhibit a linear trend indicating that linear regression is reasonable. Therefore, by applying the least-squares method to the scatter plots in figure 5 a straight line in each figure can be estimated. The estimated regression line takes the form $s = 0.60\omega_{E \times B} + 0.091$ ($\omega_{E \times B}$ scaled by 10^5) in figure 5(a) and $s = 1.47\Omega + 0.14$ in figure 5(b). The standard deviations for the slope and intercept terms are 0.14 and 0.081 in figure 5(a), respectively and 0.13 and 0.031 in figure 5(b), respectively. Relatively small values for the standard deviations of the estimators compared to the actual values of the estimators are found, thus indicating small confidence intervals for the fit and further of an accurate fit of the straight lines. Especially the curve $s = 1.47\Omega + 0.14$ shown in figure 5(b) exhibits very small relative standard deviations compared to its estimators.

The interpretation of the ITB formation in the s - Ω space could be the following: the $\omega_{E \times B}$ flow shear must be large enough to tear apart the turbulent eddies thus suppressing the long-wavelength ITG turbulence (γ_{ITG}) while at the same time small magnetic shear s

helps to disconnect the turbulent vortices (e.g. ballooning modes) initially linked together by toroidicity. Other possible mechanisms why the small magnetic shear is favourable to yield an ITB at significantly smaller $\omega_{E \times B}$ shearing rate are the splitting of some global modes [40] and some other topological modifications in the flux surface geometry [41]. This can be better understood by rearranging the terms in the estimated regression curve as $\omega_{E \times B} > s\gamma_{\text{ITG}}/1.47 - 0.14\gamma_{\text{ITG}}/1.47 = 0.68s\gamma_{\text{ITG}} - 0.095\gamma_{\text{ITG}}$. Consequently, there are two distinct regions in the s - Ω space, separated by the line $s = 1.47\Omega + 0.14$ in figure 5(b). Above the line an ITB does not exist, whereas below it an ITB does exist. The ITB is formed or collapsed, depending on the direction, when the line is crossed. The same rule is valid for all discharges in a wide B_ϕ , P_{in} and W_{dia} parameter range when the ITB is formed at typical radii in the range $\rho = 0.35$ – 0.55 . Furthermore, both the ELMy H-mode and L-mode plasmas obey the same rule, although the required Ω to compensate the magnetic shear is smaller due to smaller s at the footpoint of the ITB with an L mode edge. Moreover, the three ITB back transitions included in the analysis fit well in the same straight line.

Another point worth mentioning is the intercept term in $s = 1.47\Omega + 0.14$. A positive intercept implies that a negative or zero magnetic shear should be a sufficient condition for an ITB to exist. It is known from the theory that negative magnetic shear has a beneficial effect on curvature driven instabilities [42, 43]. Recent results from the ongoing JET experimental campaign with LHCD used also during the main heating phase to sustain negative s support the theory of the turbulence suppression, ITB formation and enhanced high performance by negative magnetic shear [44].

The time evolution of three ITB discharges in s - Ω parameter space is shown in figure 6. Diamonds, interconnected with a dotted line, indicate that no ITB yet exists whereas stars, interconnected with a dashed line, denote an existing ITB. The time interval between the consecutive points is 250–400 ms, depending on the discharge. The values of s and Ω before the ITB formation are calculated at the location where the ITB later appears. After the ITB formation the actual footpoint is followed. The thin solid lines between the last diamond and first star mark the time interval during which the ITB is formed. The thick solid line is the line $s = 1.47\Omega + 0.14$ estimated with the least-squares method, and shown in figure 5.

Both s and Ω are small at the beginning of the discharges, s because of the early phase of the current ramp-up and Ω because NBI is not yet switched on. The magnetic shear starts to increase immediately because of the current penetration. When NBI is switched on after 2–3 s, Ω also starts to increase, finally leading to the formation of the ITB. After the onset of the ITB, it typically expands in radius and goes far from the $s = 1.47\Omega + 0.14$ ITB formation threshold curve, as is the case with pulses No 47413 and 46664. Pulse No 47413 is the longest steady-state OS high performance DD discharge achieved on JET so far. Only the technical restrictions on the high power NBI system were limiting the duration of the discharge. Discharge No 47413 is a pulse with an argon puff that was used to control the ELM activity at the edge and thus, the measurements of T_i and v_ϕ have some uncertainties, further leading to larger uncertainties than normally measured by CXS in the toroidal velocity and pressure gradient (T_i) terms [45]. Pulse No 46664 has a very rapidly increasing neutron yield in the beginning, but it ends prematurely with a disruption due to the pressure-driven kink instability. The time traces of this discharge are shown in figure 1 and the radial electric field in figure 2. The empirically estimated curve $s = 1.47\Omega + 0.14$ can predict the ITB formation in s - Ω space relatively well for both discharges. However, as an opposite case to the previous pulses where full beam power were used, NBI power is decreased from 16 MW to 10 MW after the ITB formation for the shot No 48971. Therefore, the power threshold for the ITB to exist is no longer fulfilled and consequently, the ITB is lost only 1 s after its onset. This back transition is also shown in figure 6 and predicted very well by the estimated ITB formation threshold.

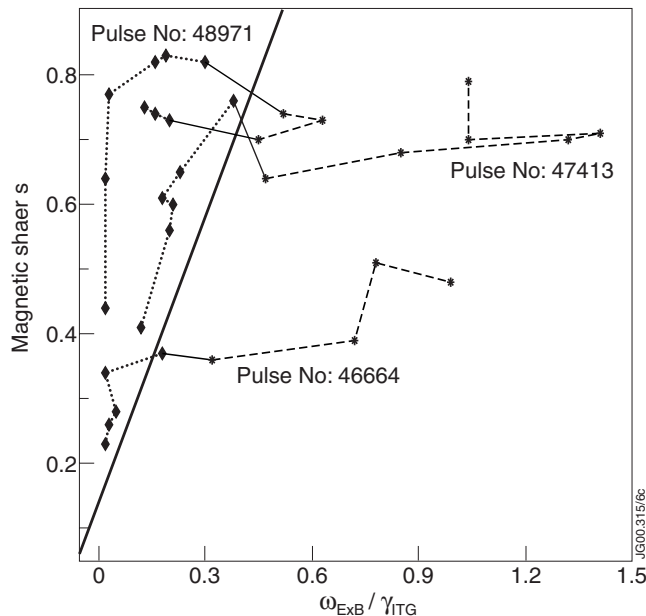


Figure 6. The time evolution of the magnetic shear as a function of Ω for 3 OS discharges. The same solid line, $s = 1.47\Omega + 0.14$, as in figure 4 is also shown.

It should be noted that in evaluation of $\Omega = \omega_{E \times B} / \gamma_{ITG}$ no account for the poloidal dependence of that quantity has been taken. As Ω here is defined, it is a flux-surface averaged quantity. Thus, the effect of Shafranov-shift is not included. However, by redefinition of $\omega_{E \times B} / \gamma_{ITG}$, its value on the outboard equator was determined and found to be about 10% larger for the present JET OS discharges than the values calculated from equation (2). Firstly due to the dominant role of ITG turbulence on JET, and secondly due to the relatively small Shafranov-shifts of JET discharges, the effect of the Shafranov-shift-induced turbulence suppression cannot be regarded as important as has been found, e.g. for the trapped electron mode turbulence in TFTR experiments [19].

4. Predictive simulations by using $s = 1.47\Omega + 0.14$ as the ITB formation condition

Predictive transport simulations of ITBs have been recently performed with several transport models and codes by many authors [22, 23, 24, 46, 47, 48]. Modelling the formation and dynamics of ITBs differs to some extent between the different transport models. At present, we will test the empirical ITB formation threshold condition $s = 1.47\Omega + 0.14$ found in section 3 for several JET OS discharges. The mixed Bohm-gyro-Bohm transport model [49] and validated in [23, 46, 49, 50] has been amended to include the ITB threshold condition. The amended set of transport coefficients can be written in the following form:

$$\chi_e = 1.0\chi_{gB} + 2.0\chi_B, \quad (3)$$

$$\chi_i = 0.5\chi_{gB} + 4.0\chi_B + \chi_i^{neo}, \quad (4)$$

$$D = [0.3 + 0.7\rho] \frac{\chi_e \chi_i}{\chi_e + \chi_i}, \quad (5)$$

where

$$\chi_{\text{gB}} = 5 \times 10^{-6} \sqrt{T_e} \left| \frac{\nabla T_e}{B_\phi^2} \right|, \quad (6)$$

$$\chi_{\text{B}} = \chi_{\text{B}_0} \times \Theta(-0.14 + s - 1.47\Omega) \quad (7)$$

and

$$\chi_{\text{B}_0} = 4 \times 10^{-5} R \left| \frac{\nabla(n_e T_e)}{n_e B_\phi} \right| q^2 \times \left(\frac{T_e(0.8\rho_{\text{max}}) - T_e(\rho_{\text{max}})}{T_e(\rho_{\text{max}})} \right). \quad (8)$$

In equations (6), (7) and (8), T_e and T_i are the electron and the ion temperatures, respectively, n_e is the electron density, B_ϕ the toroidal magnetic field, R the major radius and q is the safety factor. χ_i^{neo} is the neo-classical term for the ion heat transport [51]. The non-locality in the Bohm transport appears in the last term where ρ is the flux surface label defined by $\rho = \sqrt{\Phi/\pi B_\phi}/a_{\text{eff}}$ with a_{eff} being the radius of the circle covering the same area as the elongated plasma. ρ_{max} is the value of ρ at the separatrix in the L mode and on top of the barrier in the H mode. Φ is the toroidal magnetic flux. All the quantities appearing in equations (3)–(8) are expressed in SI units except the temperatures T_e and T_i whose unit is eV. The Θ -function multiplying the modified Bohm transport in equation (7) is the Heaviside step function with the controlling parameter given by the ITB formation threshold condition found in section 3. When the argument in the step function $-0.14 + s - 1.47\Omega = 0$ changes its sign, the ITB either forms ($\Theta(x < 0) = 0$) or collapses ($\Theta(x > 0) = 1$) as already shown in figure 5. Physically, the Bohm-type of anomalous transport χ_{B} is fully suppressed in equations (3)–(5), and the internal transport barrier forms.

The toroidal velocity is calculated from the momentum balance equation using the torque from neutral beam injection as the source term. The anomalous toroidal viscosity coefficient is assumed to be equal to the ion heat transport coefficient as in equation (4). There is experimental evidence on JET and other tokamaks that in the NB heated plasmas, the toroidal viscosity coefficient coincides with the ion heat diffusion coefficient, both radially (at least inside $r/a = 0.8$) and with time [52].

The initial and boundary conditions for the ion and electron quantities as well as the plasma current are taken from the experiment. The initial q -profile is calculated by EFIT and Z_{eff} and P_{rad} are taken from the TRANSP analysis. Also, the power deposition profiles of NBI and ICRH, and the torque are calculated by TRANSP. The standard Monte Carlo model was used for calculating the NB power deposition profiles. For the calculation of the ICRH power deposition profiles, the bounce-averaged Fokker–Planck code [53] was applied in TRANSP calculations.

The time evolution of the average ion and electron temperatures and the volume averaged electron density are shown in figure 7 for the JET OS pulse No 46664. This discharge was chosen here because it is one of the worst cases when compared to the experimental data among the analysed ITB pulses, especially in terms of the ITB formation produced by our model. Thus, it gives some insight into the order of magnitude in the maximum errors calculated by the present transport model with the ITB formation threshold condition. The temperatures, in particular the ion temperature, are overestimated by the transport model. This is due to the ITB threshold condition that triggers the ITB by 0.4 s too early for this discharge.

That the ITB is triggered too early by the model for that particular shot can be seen more clearly in the temperature profiles shown in figure 8. The first time slice at $t = 4.5$ s is before the main heating starts at $t = 5.0$ s and with an L-mode plasma edge. The L–H mode transition occurs at $t = 5.1$ s and the ITB appears at $t = 5.6$ s. However, the present transport model with the ITB threshold condition triggers the barrier already at $t = 5.2$ s, as illustrated by the

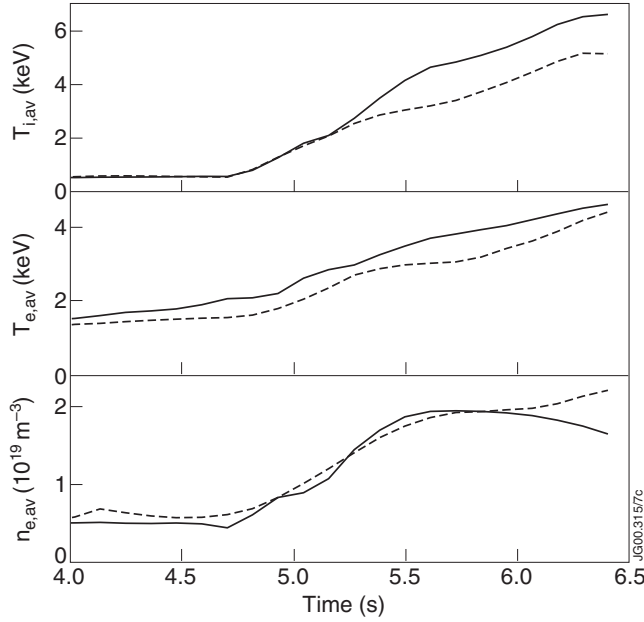


Figure 7. Reproduction of the JET discharge No 46664. Dashed curve corresponds to the experiment and solid curve is calculated by the transport model. The time evolution of the average ion and electron temperatures and the volume averaged electron density are shown.

second time slice in figure 8. Both the temperatures are overestimated and the ITB clearly exists in the simulation curves. The last two time slices describe the highest performance phase where the ITB also exists in the experiment. The model overestimates by 5–7 cm the width of the barrier at $t = 6.0$ s, but later before the disruption at $t = 6.3$ s, the location of the ITB is in agreement with the prediction.

The simulated and experimental density and toroidal velocity profiles are presented at the same instants as the temperatures in figure 9. The simulated toroidal velocity is zero at $t = 4.5$ s because the source term in the toroidal momentum balance equation in the transport model is the torque which is zero before the NBI heating.

A comprehensive predictive analysis includes several JET OS discharges from a wide plasma parameter range of $B_\phi = 1.8\text{--}4.0$ T, $P_{\text{in}} = 14\text{--}30$ MW and $W_{\text{dia}} = 3\text{--}12$ MJ. The transport model with the ITB threshold condition is identical for all the analysed discharges. To quantify the agreement between the modelling and the experiments, a statistical approach to the simulation results is applied according to the following equations:

$$\sigma_Y^2 = \sum_{i=1}^K \left(\frac{\sum_{j=1}^N [(Y_{\text{exp}}(x_j) - Y(x_j))/Y(x_j) - m_{Y,i}]^2}{N} \right) / K, \quad (9)$$

where $m_{Y,i}$ is defined as

$$m_{Y,i} = \sum_{j=1}^N \frac{(Y_{\text{exp}}(x_j) - Y(x_j))}{Y(x_j)} / N. \quad (10)$$

The quantity σ_Y^2 stands for the variance between the experimental measurement and the modelling result of the quantity Y , which can be in the present case either n_e , T_e , T_i or v_ϕ . The

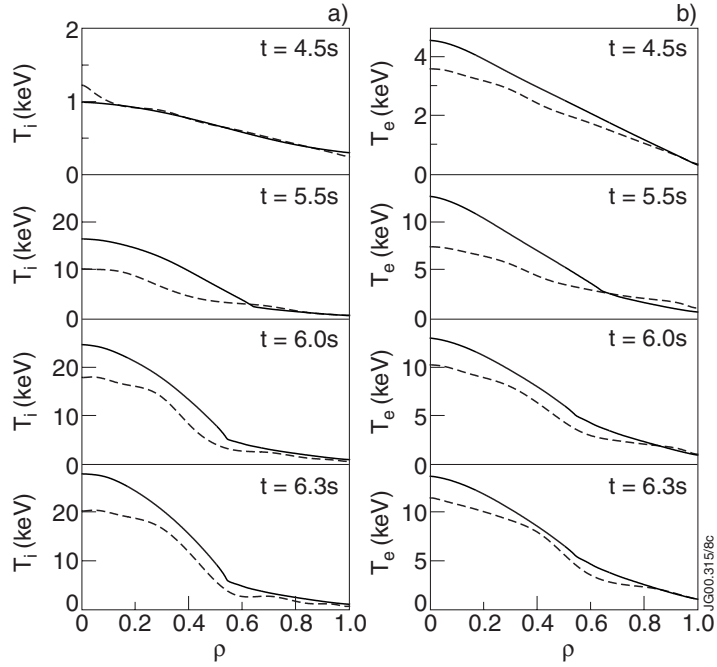


Figure 8. The ion (a) and the electron (b) temperatures at $t = 4.5$ s, $t = 5.5$ s, $t = 6.0$ s and $t = 6.3$ s. Dashed curve corresponds to the experiment and solid curve is calculated by the transport model.

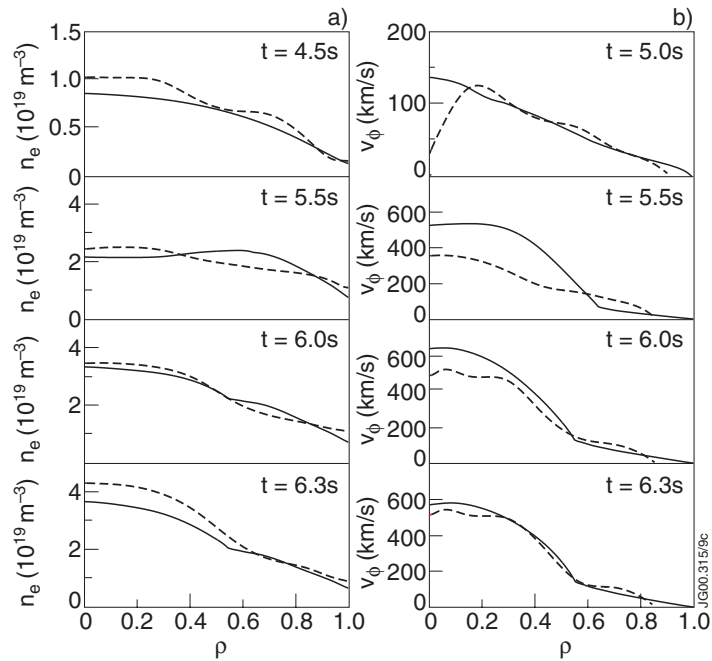


Figure 9. As in figure 8, but for density and toroidal velocity.

calculated quantity $m_{Y,i}$ symbolizes the modelling offset of the quantity Y at time t_i . The inner summation from $j = 1$ to N in equation (9) is over the radial grid points ($N = 301$) from $\rho = 0.0$ to $\rho = 0.8$ and the outer summation $i = 1$ to K is over evenly distributed K time points within the time interval of the simulation, i.e. the instants where the radial profiles have been taken. The reason for using $\rho = 0.8$ as the outermost point in the statistical analysis is that no reliable CXS measurements for v_ϕ are available beyond that radius in JET. $Y_{\text{exp}}(x_j)$ is the measured value of the given quantity at the radial point x_j and $Y(x_j)$ is the simulated one at the same point. Consequently, m_Y and σ_Y characterize the time averaged modelling offset and the time-averaged standard deviation, respectively, compared to the measured quantities over the whole duration of the simulation.

Table 1. The prediction uncertainties of the transport simulations.

| JET Pulse Number | 47843 | 49196 | 47170 | 46664 | 47413 | 46998 |
|---------------------------------------|-------|-------|-------|-------|-------|-------|
| B_ϕ [T] | 1.8 | 2.5 | 3.0 | 3.4 | 3.4 | 4.0 |
| P_{in} [MW] | 14 | 16 | 25 | 22 | 30 | 20 |
| W_{dia} [MJ] | 3 | 4 | 11 | 10 | 12 | 6 |
| Experimental ITB onset time [s] | 2.1 | 4.4 | 5.6 | 5.6 | 6.2 | 6.3 |
| Simulated ITB onset time [s] | 2.3 | 4.1 | 5.4 | 5.2 | 6.1 | 5.7 |
| Exp. ITB width at onset [r/a] | 0.42 | 0.28 | 0.50 | 0.44 | 0.53 | 0.32 |
| Sim. ITB width at onset [r/a] | 0.44 | 0.28 | 0.42 | 0.48 | 0.42 | 0.38 |
| Exp. ITB width in highest perf. [r/a] | 0.30 | 0.29 | 0.54 | 0.56 | 0.58 | 0.33 |
| Sim. ITB width in highest perf. [r/a] | 0.41 | 0.40 | 0.57 | 0.57 | 0.52 | 0.34 |
| σ_{T_i} [%] | 23 | 17 | 18 | 20 | 17 | 29 |
| σ_{T_e} [%] | 24 | 9 | 7 | 16 | 15 | 12 |
| σ_{n_e} [%] | 13 | 11 | 6 | 6 | 7 | 17 |
| σ_{v_ϕ} [%] | — | 9 | 16 | 10 | 19 | 17 |

The statistics shown in table 1 indicates that the temperature profiles T_i and T_e generally match the experimental data with prediction errors of the order of 10–25%, thus being of the same order as the experimental measurement errors that are typically within 20% in JET. The accuracy in n_e and v_ϕ profiles is even better, typically the time averaged prediction errors are in the range of 10–20%. There is also a trend that the model triggers the ITB too early (pulse No 47843 is an exception) whereas no similar trend can be observed in the width of the ITB either when it is formed or later during the highest performance phase. Furthermore, the magnitude of the overall simulation error does not depend on the magnetic field nor on any other plasma parameter.

5. Summary and discussions

The physical mechanisms of the ITB formation have been investigated with a significant number of JET OS discharges. The analysis consisted of two different parts. The first one concentrated on studying the experimental ITB data base, determination of the radial electric field and the calculation of the $\omega_{E \times B}$ flow shear and the magnetic shear. The most important result was the derivation of the empirical ITB formation threshold condition in terms of $\omega_{E \times B}$ and s . In the second part, the ITB formation condition was implemented into the JETTO transport code and the ITB formation was tested in a predictive way against several JET OS discharges from a wide plasma parameter range.

The contribution from the toroidal rotation was found to be always the dominant component in the radial electric field in JET. It produces a positive E_r with co-injected NBI, as

is typically the case in JET. When the magnetic shear was plotted as a function of the $\omega_{E \times B}$ flow shear at the onset of the ITB, a clear linear trend, i.e. the ITB formation threshold condition was found. The statistical error of this trend was smaller when the $\omega_{E \times B}$ shearing rate was divided by γ_{ITG} , thus indicating the evident role of the ITG turbulence in the ITB formation. The empirical ITB formation threshold condition takes the form $s = 1.47\omega_{E \times B}/\gamma_{ITG} + 0.14$. By rearranging the terms in the equation one obtains $\omega_{E \times B} > 0.68s\gamma_{ITG} - 0.095\gamma_{ITG}$. This empirical ITB formation condition is valid for flat, weakly positive and positive magnetic shear regions such as found in the JET OS plasmas, but not necessarily for negative magnetic shear plasmas, as is the case with NCS plasmas in DIII-D or RS plasmas in JT-60U or TFTR. The role of Shafranov-shift in the ITB formation on JET turned out to be modest, giving only about a 10% local increase in $\omega_{E \times B}/\gamma_{ITG}$ which is well within the measurement accuracy.

The physical picture of the ITB formation could be the following one: $\omega_{E \times B}$ flow shear must be large enough to tear apart the turbulent eddies thus suppressing the long wave length ITG turbulence (γ_{ITG}) while at the same time the magnetic shear s must be small enough to disconnect the turbulent vortices initially linked together by toroidicity. In addition to toroidal decoupling by small magnetic shear, it can split some global modes and can also make some other beneficial topological modifications in the flux surface geometry. It is also known from theory that negative magnetic shear has a favourable effect on curvature driven instabilities.

The comprehensive predictive analysis included several JET OS discharges from a wide plasma parameter range. The Bohm-gyro-Bohm transport model was amended with the empirical ITB formation condition in JETTO transport code. The predictive simulations reproduce the experiments with time averaged prediction errors of the order of 10–25% in T_i and T_e profiles while the uncertainties in n_e and v_ϕ are in the range of 10–20%. The simulated times of the onset of the ITB compared to the experimental ones are typically within 0.4 s and the simulated ITB widths within 0.1 in r/a throughout the whole simulations. The initial q -profile from EFIT and torque from TRANSP turned out to be the most sensitive input parameters. When the simulations are started early enough, the plasma current has enough time to evolve self-consistently and, as a consequence, the sensitivity to the initial q -profile can be eliminated. The sensitivity of the simulation predictions on the slope (=1.47) in the ITB formation condition $s = 1.47\omega/\gamma_{ITG} + 0.14$ was rather weak. By increasing or decreasing the slope by 40%, advanced or delayed, respectively, the ITB formation time by 0.10–0.25 s, and correspondingly the width of the ITB by 0.05–0.10 in r/a . The sensitivity on the intercept term (= 0.14) was somewhat larger.

Future efforts will be aimed at extending the model to include a treatment of the ETG mode, which may affect the electron transport [54]. In the present work, the ITB formation threshold condition was derived mainly from the ion transport channel, but the same ITB triggering condition was also applied to the electron transport. However, it is likely that the electron temperature profiles would be in better agreement with experiments when the ion and electron transport channels are separated. An important and useful way to proceed in future is to test the ITB formation threshold condition found in this study for discharges from other tokamaks where the plasma parameters and experimental settings, in particular the magnetic shear, are similar to that of the present JET OS operation mode.

Acknowledgments

The authors are grateful to Claude Gormezano for many fruitful discussions during the project. The authors also thank Arthur Peeters for giving useful ideas on approaching the problem. We are also grateful to Carine Giroud for her help in the calculation of the rotation velocities. Special thanks also belong to David Heading and Gerard Corrigan for technical assistance.

References

- [1] Levinton F M *et al* 1995 *Phys. Rev. Lett.* **75** 4417
- [2] Rice B W *et al* 1996 *Phys. Plasmas* **3** 1983
- [3] Fujita T *et al* 1997 *Phys. Rev. Lett.* **78** 2377
- [4] Söldner F X *et al* 1999 *Nucl. Fusion* **39** 407
- [5] Staebler G M 1998 *Plasma Phys. Control. Fusion* **40** 569
- [6] Diamond P H *et al* 1997 *Phys. Rev. Lett.* **78** 1472
- [7] Ernst D R *et al* 1998 *Phys. Rev. Lett.* **79** 2454
- [8] Synakowski E J 1998 *Plasma Phys. Control. Fusion* **40** 581
- [9] Shirai H *et al* 2000 *Plasma Phys. Control. Fusion* **42** A109
- [10] Baranov Yu F *et al* 1999 *Nucl. Fusion* **39** 1463
- [11] Gruber O *et al* 2000 *Plasma Phys. Control. Fusion* **42** A117
- [12] Strait E J *et al* 1995 *Phys. Rev. Lett.* **75** 4421
- [13] The JET Team *Plasma Phys. Control. Fusion* **39** B353
- [14] Koide Y 1998 *Plasma Phys. Control. Fusion* **40** 641
- [15] Burrell K H 1997 *Phys. Plasmas* **4** 1499
- [16] Challis C D *et al* 2001 Effect of q -profile modification by LHCD on internal transport barriers in JET *Plasma Phys. Control. Fusion* submitted
- [17] Challis C D *et al* 1999 *Proc. 26th European Physical Society Conf. on Controlled Fusion and Plasma Physics (Maastricht, The Netherlands, 14–18 June, 1999) (ECA vol 23J)* p 69
- [18] Hogeweijs G M D *et al* 1998 *Nucl. Fusion* **38** 1881
- [19] Synakowski E J *et al* 1997 *Phys. Rev. Lett.* **78** 2972
- [20] Hahm *et al* 2000 *Plasma Phys. Control. Fusion* **42** A205
- [21] Conway G D *et al* 2000 *Phys. Rev. Lett.* **84** 1463
- [22] Zhu P *et al* 2000 *Phys. Plasmas* **7** 2898
- [23] Parail V V *et al* 1999 *Nucl. Fusion* **39** 429
- [24] Kinsey J E *et al* 1999 *Proc. 26th European Physical Society Conf. on Controlled Fusion and Plasma Physics (Maastricht, The Netherlands, 14–18 June, 1999) (ECA vol 23J)* p 1205
- [25] Hahm T S and Burrell K H 1995 *Phys. Plasmas* **2** 1648
- [26] Hamaguchi S and Horton W 1992 *Phys. Fluids B* **4** 319
- [27] Weiland J and Hirose A 1992 *Nucl. Fusion* **32** 151
- [28] Lao L *et al* 1985 *Nucl. Fusion* **25** 1611
- [29] Genacchi G and Taroni A 1988 JETTO: A free boundary plasma transport code (basic version) *Rapporto ENEA RT/TIB* 1988(5)
- [30] Tresset G, Litaudon X and Moreau D 2000 A dimensionless criterion for characterising internal transport barriers in tokamaks *Report DRFC/CAD EUR-CEA-FC-1700* July 2000
- [31] Rozhansky V and Tendler M 1992 *Phys. Fluids B* **4** 1877
- [32] Shaing K C *et al* 1999 *Phys. Rev. Lett.* **83** 3840
- [33] Kim J *et al* 1994 *Phys. Rev. Lett.* **72** 2199
- [34] Staebler G M, Waltz R E and Wiley J C 1997 *Nucl. Fusion* **37** 287
- [35] Greenfield C M *et al* 2000 *Phys. Plasmas* **7** 1959
- [36] Synakowski E J *et al* 1999 *Nucl. Fusion* **39** 1733
- [37] Doyle E J *et al* 2000 *Proc. 18th IAEA Fusion Energy Conference (Sorrento, 4–10 October, 2000) IAEA-CN-77/EX6/2*
- [38] Sakamoto Y *et al* 2000 *Proc. 18th IAEA Fusion Energy Conference (Sorrento, 4–10 October, 2000) IAEA-CN-77/EX6/4*
- [39] Nordman H, Weiland J and Jarmen A 1990 *Nucl. Fusion* **30** 983
- [40] Kishimoto Y *et al* 1998 *Plasma Phys. Control. Fusion* **40** A663
- [41] Beer M A *et al* 1997 *Phys. Plasmas* **4** 1792
- [42] Sydora R D *et al* 1996 *Plasma Phys. Control. Fusion* **38** A281
- [43] Dong J Q *et al* 1996 *Phys. Plasmas* **3** 3065
- [44] Challis C D *et al* 2001 *Proc. 28th European Physical Society Conf. on Controlled Fusion and Plasma Physics (Madeira, Portugal, 18–22 June, 2001)* in press
- [45] Zastrow K-D *et al* 1999 *Proc. 26th European Physical Society Conf. on Controlled Fusion and Plasma Physics (Maastricht, The Netherlands, 14–18 June, 1999) (ECA vol 23J)* p 217
- [46] Tala T J J *et al* 2000 *Nucl. Fusion* **40** 1635
- [47] Pereverzev G *et al* 1999 *Proc. 26th European Physical Society Conf. on Controlled Fusion and Plasma Physics*

- (Maastricht, The Netherlands, 14–18 June, 1999) (ECA vol 23J), p 1429
- [48] Voitsekhover I *et al* 1999 *Proc. 26th European Physical Society Conf. on Controlled Fusion and Plasma Physics (Maastricht, The Netherlands, 14–18 June, 1999)* (ECA vol 23J), p 957
- [49] Erba M *et al* 1997 *Plasma Phys. Control. Fusion* **39** 261
- [50] Erba M *et al* 1996 Validation of a new mixed Bohm/gyro-Bohm transport model on discharges of the ITER data-base *JET Report JET-R(96)07*
- [51] Hinton F L, Hazeltine R D 1976 *Rev. Mod. Phys.* **48** 239
- [52] de Esch H P L, Stork D, Weisen H 1990 *Proc. 17th European Physical Society Conf. on Controlled Fusion and Plasma Physics (Amsterdam, The Netherlands, 25–29 June, 1990)* (ECA vol 14B) p 90
- [53] Smithe D N *et al* 1989 *Proc. 8th Topical Conf. on Radio-Frequency Power in Plasmas (AIP, New York)* p 338
- [54] Jenko F *et al* 2000 *Phys. Plasmas* **7** 1904